Acta Cryst. (1988). A44, 8-14

X-ray Topography of Bent Crystals

BY F. N. CHUKHOVSKII

Institute of Crystallography, Academy of Sciences of the USSR, Leninsky prospekt 59, Moscow, USSR

AND P. V. PETRASHEN'

VNII Nauchpribor, Leningrad, USSR

(*Received* 18 *November* 1986; *accepted* 20 *May* 1987)

Abstract

The influence of the bending of a crystal on the formation of diffracted images in Bragg section topographs as well as in Laue section and traverse topographs is studied. In the case of Bragg section topography the interferometric fringes due to the interference of waves once and twice internally reflected inside a bent crystal are described. It is established that the maximum positions of diffracted intensity satisfy the law $x_n = [16\pi(2n-1)/5B^2]^{1/3}$, where x_n is the distance from the incidence slit of the X-rays, B is the uniform strain gradient and n is the fringe number. This dependence is found to be in good agreement with experimental data. The Laue section topograph of a bent crystal with a screw dislocation parallel to the diffraction vector is considered. The effects of asymmetry in the *Pendellösung* fringe pattern and of 'splitting' of the direct image with respect to the dislocation line in both the experimental and simulated topographs are accounted for. The variation of the contrast of dislocations with depth inside a bent crystal in Laue traverse topographs is studied by computer simulations using the reciprocity theorem.

1. Introduction

The dynamical scattering of X-rays (DSXR) in distorted crystals with a uniform strain gradient (USG) has been investigated in a number of studies (Kato, 1964; Bonse, 1964; Penning, 1966; Hart, 1966; Blech & Meieran, 1967; Malgrange, 1969; Ando & Kato, 1970; Petrashen', 1973; Chukhovskii, 1974; Petrashen' & Chukhovskii, 1975; Chukhovskii & Petrashen', 1977; Chukhovskii, Gabrielyan & Petrashen', 1978; Kushnir, Suvorov & Mukhin, 1980; Khrupa, Kislovskii & Datzenko, 1980; Petrashen' & Yaroslavskaya, 1981; Balibar, Chukhovskii & Malgrange, 1983; Shulpina, Petrashen', Chukhovskii & Gabrielyan, 1984) and is a starting point for the quantitative theory of X-ray topographic images and the theory of DSXR in distorted crystals in general.

In practice a situation can exist where the USG macroscopic elastic field is superposed on those caused by single defects in a crystal. Their cooperative action was experimentally observed: in X-ray traverse topographs of bent crystals the dislocation contrast is found to be reversed (Blech & Meieran, 1967); in Laue section topographs of a twisted silicon crystal the *Pendellösung* fringe patterns become asymmetrical with respect to a dislocation line (Kushnir, Suvorov & Mukhin, 1980); owing to dislocation loops randomly distributed within a crystal the dependence of the reflecting power on the radius of curvature of the sample is changed (Khrupa, Kislovskii & Datenzko, 1980); and in Bragg diffraction a new kind of USG fringe, curved near local inhomogeneities, has been observed recently (Shulpina, Petrashen', Chukhovskii & Gabrielyan, 1984).

The study of these phenomena is of interest in itself since it permits one to understand better the general features of the formation of X-ray topographic images and it can also demonstrate how to use crystal bending as a new tool for DSXR investigations of crystal-lattice defects.

In the present paper we shall discuss the physical foundations of the formation of X-ray topographic images for bent crystals; these are important from the point of view of applications and further development of DSXR methods. We confine our consideration to the case of the USG $|B| \ll 1$ [the dimensionless USG $B = \frac{1}{4}\partial^2(\mathbf{hu})/\partial s_0 \partial s_h$; hereafter the notation is that of Petrashen' & Chukhovskii (1975)], when two wave fields relating to the two branches of the dispersion surface are essential and contribute simultaneously to the formation of images. In § 2 the Green function of the diffracted radiation and its asymptotic expression (the eikonal approximation) are used for the explanation of the *Pendellösung* fringes in Laue section topographs. The eikonal approximation is used to treat the USG fringe formation in Bragg section topographs in § 3.

In the final section some pecularities of the dislocation images in both Laue section and traverse topographs are discussed. The treatment is based on

0108-7673/88/010008-07$03.00

computer-simulated images calculated with a numerical variable-step algorithm (Petrashen', 1976) and the reciprocity theorem (Petrashen', Chukhovskii & Shulpina, 1980).

2. *Pendellösung* fringes in Laue section topographs

The general theory of DSXR in a crystal with an arbitrary USG is developed by Chukhovskii & Petrashen' (1977), using the Green-function method. In the case of $|B| \ll 1$ for the Green function of the diffracted radiation one has the following expression in the entire region of influence $\rho = 2(s_0 s_h)^{1/2} \geq 0$ (the so-called Borrmann fan):

$$G_{h0}(s_0, s_h) \simeq J_0[S(\rho)] \tag{2.1}$$

with the eikonal function

$$\begin{aligned} S(\rho) = {} & (\rho/2)(1+B^2\rho^2)^{1/2} \\ & + [(1+2ik)/2|B|] \ln[(1+B^2\rho^2)^{1/2} + |B|\rho] \\ & - i\varepsilon \ln[(1+B^2\rho^2)^{1/2} + |B|\rho], \end{aligned} \tag{2.2}$$

where $\varepsilon = \text{sign } B$, $J_0(S)$ is the Bessel function of zero order, and k is the normalized dynamical absorption coefficient, $k < 0$.

The first and second terms on the right-hand side of (2.2) are completely equivalent to the Kato eikonal (Kato, 1964). The third term in (2.2) is included in the amplitude of the diffracted wave in the Kato theory. The eikonal function (2.2) was fruitfully utilized for experimental studies of *Pendellösung* fringes in elastically deformed silicon (Hart, 1966) and the penetration of two wave fields through silicon crystals deformed by a uniform temperature gradient (Malgrange, 1969).

As is seen from (2.2) the imaginary part of the eikonal function depends on the strain sign $\varepsilon = \text{sign } B$ through the parameter $k/|B| - \varepsilon$. The transition from the dynamical coefficient k to $k - B$ can be interpreted as the renormalization of the dynamical absorption for any USG [for details, see Chukhovskii & Petrashen' (1977)].

In accordance with (2.1) and (2.2) the wave-front surfaces within the Borrmann fan are the hyperbolic cylinders $\rho = \text{constant}$, similar to the case of a perfect crystal. The *Pendellössung* fringe positions in the Laue section topograph are determined by the phase difference between the two wave fields $\Delta\Gamma = 2 \text{ Re } S$ and now depend on the USG parameter B. A numerical example of the phase difference $\Delta\Gamma$ *versus* the strain parameter $\mathcal{D} = BT$ along the section topograph axis $x = 0$ (T is the dimensionless crystal thickness) is shown in Fig. 1.

From (2.1) and (2.2) it follows that the *Pendellösung* fringe positions do not depend on the USG sign while their contrast does so, owing to the renormalization of the dynamical absorption coefficient $k \to k - B$. In Fig. 2 the integrated reflecting-power coefficients of the two wave fields as functions of the USG parameter B are drawn. It is easily seen that they are equal to each other at the point $B = k$. In this case the *Pendellösung* fringe contrast is maximum and the total integrated reflecting power falls to a minimum.

It is worth noticing that the phase difference $\Delta\Gamma' = \Delta\Gamma(B \neq 0) - \Delta\Gamma(B = 0) < 1$ for $|B| < T^{-3/2}$ [see (2.2)] and for the diffracted wave field the influence of the crystal bending reduces only to the renormalization of the dynamical absorption coefficient.

In the general case of an arbitrary distortion of the crystal lattice the exact solution for the Green function of the problem in question is not known. Nevertheless, one can write down a simple formula for the phase of the diffracted wave along the section-topograph axis ($x = 0$), using the equation for the eikonal function

$$(\partial S/\partial z - \alpha)^2 - (\partial S/\partial x + \alpha)^2 = 1 + 2ik, \tag{2.3}$$

where the deviation parameter $\alpha(x, z)$ at a point (x, z) inside a crystal is defined as

$$\begin{aligned} \alpha(x, z) &= (\alpha_0/4|\gamma_h|) - \tfrac{1}{2}\partial(\mathbf{hu})/\partial s_h, \\ \alpha_0 &= (K_h^2 - K_0^2)/K_0^2. \end{aligned} \tag{2.4}$$

Assuming that the eikonal function $S(x, z)$ mainly depends on the hyperbolic coordinate $\rho = (z^2 - x^2)^{1/2}$ and neglecting the derivative $\partial S/\partial x$ in comparison

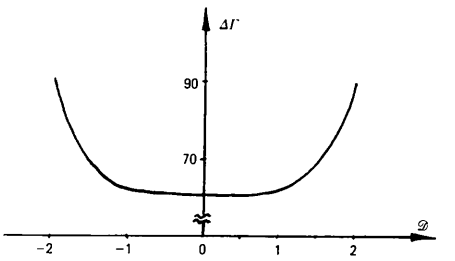

Fig. 1. The dependence of the phase difference $\Delta\Gamma$ on the strain $\mathcal{D} = BT$; T is the dimensionless crystal thickness, $T = 30$.

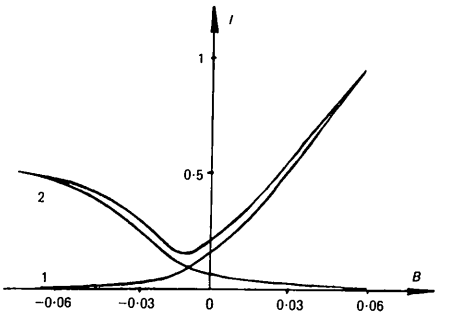

Fig. 2. The total integrated intensity I and its components relating to the Bloch waves *versus* the strain gradient B. Si crystal, Mo $K\alpha$, 311 reflection, $T = 30$, $k = -0{\cdot}01$.

with $\partial S/\partial z$ one can find, from (2.3),

$$S(0, z)=\int_0^z dz'\{\alpha[0, z'\pm(1+2ik+\alpha^2(0, z')]^{1/2}\}. \tag{2.5}$$

It is interesting that in the case of a crystal with USG the approximate formula (2.5) seems to provide the same result for the phase difference $\Delta\Gamma(0, z)$ as does the exact solution of the problem.

We shall use (2.5) further to analyse the features of the *Pendellösung* fringe pattern in Laue section topographs of dislocations in a bent crystal.

3. A new kind of interfermometric fringe in Bragg section topographs

In the Bragg geometry of X-ray diffraction in a crystal with USG the section-topograph pattern is described with the Green function introduced by Chukhovskii, Gabrielyan & Petrashen' (1978). The expansion of this function as a wave packet takes the form

$$G_{h0}\sim\int_{P_0-i\infty}^{P_0+i\infty} dp\, P_h(p), \tag{3.1}$$

where

$$P_h(p)=\frac{1}{2\pi}\nu^{1/2}\frac{\mathcal{D}_{-1-\nu}(-iY)}{\mathcal{D}_{-\nu}(-iY_0)}\exp[(p/2)(s_0+s_h)]. \tag{3.2}$$

Here the parameters Y_0 and Y are such that

$$Y_0=i\nu^{1/2}p, \tag{3.3}$$

$$Y=Y_0+4\nu^{1/2}B(s_0+s_h), \tag{3.4}$$

and $\mathcal{D}_\nu$ is the parabolic cylinder function of order ν equal to

$$\nu=i(1+2ik)/4B. \tag{3.5}$$

An analysis of wave-field propagation in the bulk of a crystal can be carried out on the basis of (3.1)–(3.5), like the analysis performed by Balibar, Chukhovskii & Malgrange (1983) (see also Chukhovskii, Gabrielyan & Petrashen', 1978; Chukhovskii, 1981; Gronkowski & Malgrange, 1984) in the Laue diffraction case; it yields the following picture.

According to the well known Ewald–Laue theory an incident spherical wave generates two wave fields below the entrance surface of a crystal. In a semi-infinite crystal only the Bloch waves belonging to the lower part of branch 1 ($\alpha_0>0$) and the upper part of branch 2 ($\alpha_0<0$) of the dispersion surface are excited (Fig. 3). Correspondingly, the Bloch waves of type 1 (2) are damped exponentially in the bulk of a crystal with the USG $B<0$ ($B>0$) and, hence, do not contribute to the image while the waves of type 2 (1) propagating along hyperbolic trajectories undergo internal reflection at a depth $z_*=\frac{1}{4}(|\alpha_0|/|\gamma_h B|-2/|B|)$ inside a crystal and then return to the entrance surface. Here they are split into two parts, the outgoing and reflected waves, and so the process continues (Chukhovskii, Gabrielyan & Petrashen', 1978). In other words, wave-field components with sign $(\alpha_0\beta)>0$ gain the capability of a 'waveguide' travelling along the entrance surface over large distances, restricted only by their absorption lengths. As a consequence, a new kind of interferometric fringe seems to be possible owing to the interference of the Bloch waves coming to a given point on the entrance surface as a result of a number of successive internal reflections. Physically it is clear that it is the waves which undergo internal reflections repeated once and twice that mainly contribute to fringe formation (Fig. 4).

The eikonal function of a once-reflected wave is determined by the same expression as in the Laue diffraction case, (2.2), with the substitution $x\rightleftarrows z$. Hence, at the point $(x, 0)$ on the entrance surface one has

$$\begin{aligned}\Gamma_1(x)&=\mathrm{Re}\, S_1(x)\\&=x/2(1+B^2x^2)^{1/2}\\&\quad+(1/2|B|)\ln[(1+B^2x^2)^{1/2}+|B|x].\end{aligned} \tag{3.6}$$

Correspondingly, for the doubly reflected wave the eikonal function is equal to

$$\Gamma_2(x)=2\Gamma_1(x/2)-\pi, \tag{3.7}$$

where $-\pi$ is the phase shift due to the reflection of the Bloch wave from the entrance surface.

As is easily seen, for small values of x the phase difference $\Delta\Gamma=\Gamma_1-\Gamma_2\simeq\pi$ and fringe formation is suppressed. The first and subsequent fringes occur provided that the condition

$$\Gamma_1(x_n)-\Gamma_2(x_n)=2\pi n \tag{3.8}$$

is satisfied, beginning with the number $n=1$.

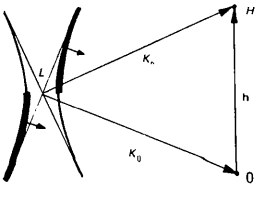

Fig. 3. The initial excitation points of the Bloch waves on the dispersion surface. The Bragg diffraction case.

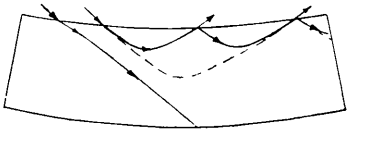

Fig. 4. Ray trajectories in a bent crystal. The Bragg diffraction case.

Supposing that $|B|x<1$ (one recalls that $|B|\ll 1$) and taking into account (3.6)–(3.8), one can find a simple estimate for the positions of fringe maxima:

$$x_n=[16\pi(2n-1)/5B^2]^{1/3}. \qquad (3.9)$$

USG fringes in Bragg section topographs thus appear, starting from the 'threshold' length. The first fringe is at a distance $x_1=(16\pi/5B^2)^{1/3}$ from the incidence slit and subsequent ones are located in accordance with the law $x_n\simeq(n-\frac{1}{2})^{1/3}$.

These fringes were experimentally observed by Shulpina, Petrashen', Chukhovskii & Gabrielyan (1984). A topograph and its microdensitometric curve are shown in Figs. 5 (*a*) and (*b*). The theoretical and experimental dependences of x_n^3 as functions of the number n are plotted in Fig. 5(*c*). It is seen that theory and experiment are in good agreement. The slope of the straight line x_n^3 is proportional to B^{-2} [see (3.9)] and from here a simple method for USG-value determination evidently follows.

As an example the fringe pattern for a crystal with the strain gradient varying along the direction perpendicular to the diffraction plane is represented in Fig. 6. The simulation is performed by means of the numerical solution of the Takagi–Taupin equations. It is clearly seen that the fringe contrast depends on the USG sign just as in the Laue diffraction case. The reason is that the USG sign defines the Bloch waves which form the fringe pattern. They are the weakly (strongly) absorbing waves relating to branch 1 (2) of the dispersion surface for $B>0$ ($B<0$). Therefore, the fringe contrast and its reduction as the distance from the incidence slit increases are not symmetrical with respect to the line $B=0$ (see Fig. 6).

It is essential that for small USG values the first distance x_1, which increases as $B^{-2/3}$ [see (3.9)], can become larger than the X-ray absorption length $x_{\rm abs}=\mathscr{C}|\beta\ \mathrm{Re}\,(\chi_h\chi_{-h})|^{1/2}/\mathrm{Im}\,\chi_0(1+|\beta|)$, $\beta=\gamma_0/\gamma_h$. Then, one has the critical value of the USG

$$|B|_{\rm cr}=(16\pi/5x_{\rm abs}^3)^{1/2}, \qquad (3.10)$$

below which the fringe contrast is negligible.

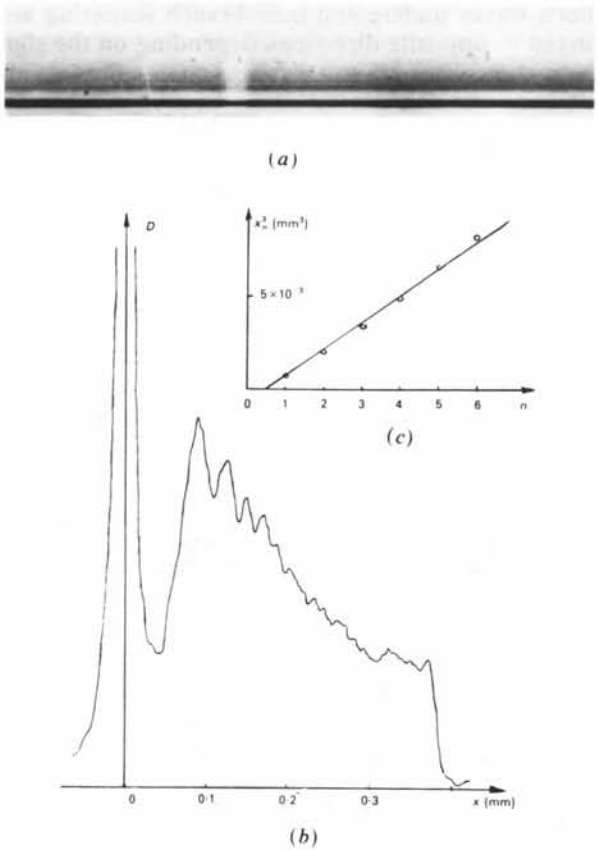

Fig. 5. The Bragg section topograph of a bent crystal. (Si crystal, radius of curvature $R=60$ m, Mo $K\alpha$, 333 reflection. Courtesy I. L. Shulpina.) (*a*) Experimental image, (*b*) microdensitometric curve, (*c*) positions of the diffracted intensity maxima as a function of the fringe number.

4. The Laue section and traverse images of dislocations

In order to exhibit the main features of images of single dislocations in bent crystals let us assume for simplicity the Laue symmetrical diffraction case and a screw dislocation parallel to the crystal surface, such that

$$(\mathbf{hu})=[(\mathbf{hb})/2\pi]\ \mathrm{arc\ tan}\ (z-z_0)/y, \qquad (4.1)$$

$$\alpha_d=-[(\mathbf{hb})/4\pi]y/[y^2+(z-z_0)^2]. \qquad (4.2)$$

Here $\mathbf{h}$ is the diffraction vector, $\mathbf{b}$ is the Burgers vector, z_0 and y are the depth of a screw dislocation and the coordinate perpendicular to the diffraction plane, respectively.

Bearing in mind that we want to treat the cooperative influence of strains caused by the bend and by the dislocation on *Pendellösung* fringe formation we shall use (2.5) for the eikonal function $S(0, z)$.

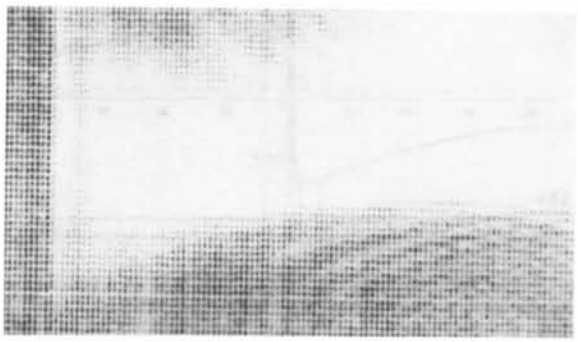

Fig. 6. The simulated Bragg section topograph of a bent crystal. The strain gradient B varies from $B=-4$ in the upper part to $B=4$ in the lower part of the image. Si crystal, Cu $K\alpha$, 444 reflection.

In our case the total deviation parameter $\alpha(0, z)$ is equal to [*cf.* (4.2)]

$$\alpha(0, z) = -Bz - [(\mathbf{hb})/4\pi]y/[y^2 + (z - z_0)^2]. \quad (4.3)$$

Substituting (4.3) into (2.5) one easily finds the maximum phase difference for the limit $y \to 0$,

$$\Gamma(0) = \Delta\Gamma_b + |(\mathbf{hb})|/2, \quad (4.4)$$

where $\Delta\Gamma_b$ is the phase difference due to the bend of the crystal only.

For arbitrary values of y the function $\Delta\Gamma(y)$ is complicated and depends on the sign of the product $yB(\mathbf{hb})$. The behaviour of $2\Delta\Gamma(y) - \pi/2$ *versus* y and the corresponding schematic image of the central *Pendellösung* fringe contrast in the Laue section topograph of the screw dislocation with $(\mathbf{hb}) = -4\pi$ are shown in Figs. 7(*a*) and (*b*), respectively. It is seen that when $|y|$ decreases the curve $2\Delta\Gamma(y) - \pi/2$ increases monotonically under the condition that $yB(\mathbf{hb}) > 0$, whereas for $yB(\mathbf{hb}) < 0$, $2\Delta\Gamma(y) - \pi/2$ first decreases, coming to a minimum at the point $|y| = |(\mathbf{hb})/4\pi Bz_0|$, and then it tends to the maximum given by (4.4). This is the reason for the asymmetry of the *Pendellösung* fringe pattern with respect to the dislocation line $y = 0$ observed in the experimental and simulated section topographs of Figs. 8(*b*) and (*d*).

From this the simple rule for the determination of the Burgers-vector sign of a dislocation under the bending of a crystal evidently follows.

It is worth noticing that in the case of a bent crystal the sensitivity of the *Pendellösung* fringe pattern to small strain fields enlarges. Indeed, as is seen from Fig. 7(*a*) a noticeable change of $\Delta\Gamma$ takes place over distances of the order of ten extinction lengths from a dislocation line. The reason is that for $B = 0$ the phase difference $\Delta\Gamma$ as a function of B has a minimum $[\partial(\Delta\Gamma)/\partial B|_{B=0} = 0]$, while if $B \neq 0$ then $\partial(\Delta\Gamma)/\partial B \neq 0$, and hence the local strain gives rise to a linear contribution to the phase difference $\Delta\Gamma$.

Now let us consider another new interesting effect, namely the 'splitting' of direct images of a dislocation in the bent crystal with respect to the dislocation line (see Figs. 8*b*, *d*). To understand the nature of this phenomenon it is necessary to remember that a direct image is formed as a result of the inter-branch scattering of the Bloch waves in the area of the intersection of the dislocation line with the incident X-ray beam direction. These Bloch waves have initial excitation points lying on different branches of the dispersion surface: on branch 1 for $\alpha_0 > 0$ and on branch 2 for $\alpha_0 < 0$, as shown in Fig. 9. In the case in question, for a fixed sign of the dislocation deviation parameter α_d only one of the two Bloch waves undergoes inter-branch scattering near the dislocation line, where its excitation point passes through the central region of the dispersion surface. A subsequent analysis shows that, for the dislocation side $y(\mathbf{hb}) > 0$ or $y(\mathbf{hb}) < 0$, so the Bloch wave belongs to either branch 1 or branch 2, respectively. For bent crystals trajectories of the Bloch waves undergoing inter-branch scattering are curved in opposite directions depending on the sign

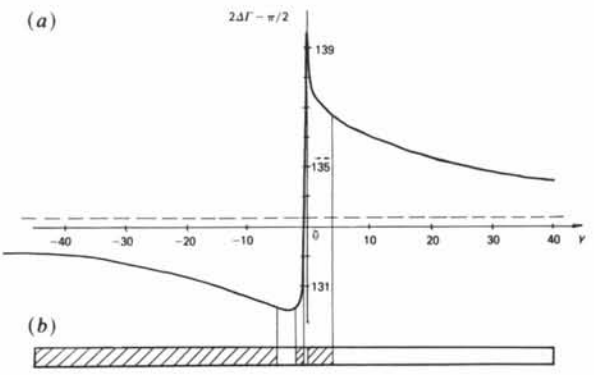

Fig. 7. (*a*) The phase difference $2\Delta\Gamma(y) - \pi/2$ as a function of the distance y from the screw dislocation with $(\mathbf{hb})/2\pi = -2$ along the axis of the Laue section topograph. $T = 51{\cdot}68$, $B = -0{\cdot}0293$ (Si crystal, Mo $K\alpha$, 220 reflection, crystal thickness $t = 600$ μm). (*b*) Schematic image of the central *Pendellösung* fringe in the Laue section topograph, drawn in accordance with $2\Delta\Gamma(y) - \pi/2$ in (*a*). The dashed line shows the asymptotic value of $2\Delta\Gamma(y) - \pi/2$ for $|y| \to \infty$.

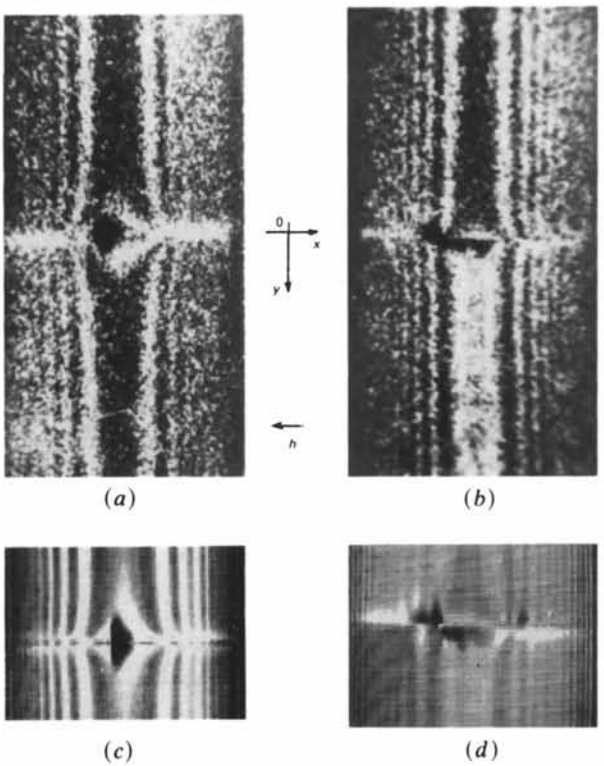

Fig. 8. The experimental (*a*), (*b*) and simulated (*c*), (*d*) Laue section topographs of an Si crystal with a screw dislocation (courtesy E. V. Suvorov). Mo $K\alpha$, 220 reflection, $t = 600$ μm, $(\mathbf{hb})/2\pi = -2$; (*a*), (*c*) $B = 0$, (*b*), (*d*) $B = -0{\cdot}0293$.

of the USG parameter B. This means that on both sides of the dislocation marked by the sign of $y\boldsymbol{B}(\mathbf{hb})$ the parts of the direct image are shifted in opposite directions with respect to each other, and as a consequence the determination of the sign of the Burgers vector is feasible. In particular, in Figs. 8(b) and (d) $(\mathbf{hb})<0$, if one recalls the formula (4.1) for the displacement function of reflecting planes due to a screw dislocation and that the USG parameter $B<0$.

In conclusion, we shall briefly discuss several pecularities of traverse images of dislocations in bent crystals. *A priori*, it is clear that in the case under consideration the interference of the Bloch waves belonging to different branches of the dispersion surface is not very important. We restrict ourselves to USG values for which the condition

$$B^2T^3<3\pi \tag{4.5}$$

holds, so that the phase difference $\Delta\Gamma'=\Delta\Gamma(B\neq 0)-\Delta\Gamma(B=0)$ due to the bending of a crystal is smaller than π [see (2.2)]. Besides, the case of the Lang contrast of images is of practical interest when $2|k|T\lesssim 1$.

In this case, only the effect of renormalization of the dynamical absorption coefficient $k\to k-B$ is essential. Therefore the bending of a crystal with the USG parameter $B>0$ makes the effective dynamical absorption of X rays larger, and the transition from the Lang contrast of images to the Borrmann one takes place.

In order to illustrate this conclusion the simulated traverse images of the screw dislocations $I(y)$ with different depths under the entrance surface of a crystal are plotted in Fig. 10 ($B=0$) and Fig. 11 ($B\neq 0$). The simulations were performed by use of the numerical variable-step algorithm proposed by Petrashen' (1976) and the reciprocity theorem (Petrashen', Chukhovskii & Shulpina, 1980).

As can be seen from Fig. 10, dislocation image profiles $I(y)$ have two peaks. At the point $y=0$ the dislocations are not visible since the product $(\mathbf{hb})/2\pi=2$ is even. For dislocations lying near either the entrance or exit surface the intensity peaks have different heights on both sides of the line $y=0$. Physically, this is connected with the circumstance pointed out above. The direct image is formed owing to the inter-branch scattering of Bloch waves of either type 1 or type 2 depending on the sign of the product $y(\mathbf{hb})$. These Bloch waves have different paths above and below the dislocation line, with the exception of the dislocation lying in the middle of a crystal, for which the wave field forming a direct image is, on the average, absorbed normally.

A comparison of Figs. 10 and 11 confirms the main theoretical conclusion that for the USG $B>0$ the enhancement of the effective dynamical absorption of X-rays in bent crystals yields the Borrmann kind of image contrast for any depth of dislocation under the entrance surface, although the asymmetry of profiles owing to the dominant contribution by one of the two Bloch waves is, in general, conserved. In the opposite case of the USG $B<0$ the dislocation image contrast is positive as a whole and it is similar to that for a non-absorbing flat crystal.

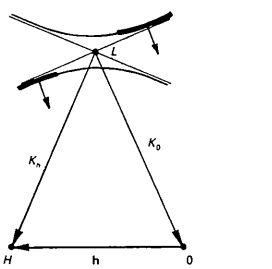

Fig. 9. The initial excitation points of the Bloch waves forming the direct image of a dislocation.

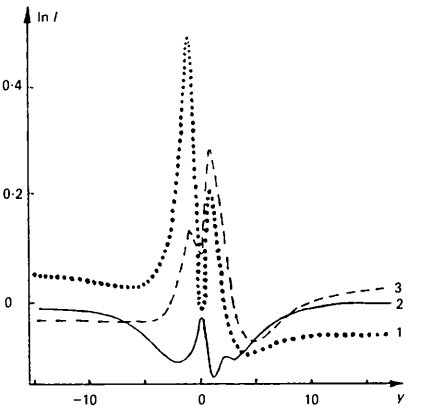

Fig. 10. The simulated profiles of traverse images of screw dislocations in a flat crystal ($B=0$); $T=30$, $(\mathbf{hb})/2\pi=2$, $z_0=$ (1) 5, (2) 15, (3) 25; Cu $K\alpha$, $k=-0{\cdot}05$.

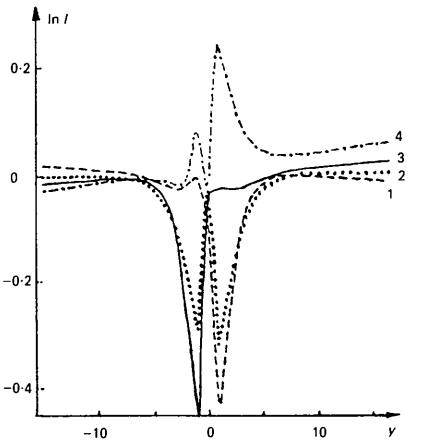

Fig. 11. The same as in Fig. 10 for a bent crystal. (1)–(3) $B=0{\cdot}05$, (4) $B=-0{\cdot}05$, $z_0=5$.

The authors are greatly indebted to I. L. Shulpina and E. V. Suvorov for the experimental topographs placed at their disposal.

References

ANDO, Y. & KATO, N. (1970). *J. Appl. Cryst.* **3**, 74-89.

BALIBAR, F., CHUKHOVSKII, F. N. & MALGRANGE, C. (1983). *Acta Cryst.* A**39**, 387-399.

BLECH, I. A. & MEIERAN, E. S. (1967). *J. Appl. Phys.* **38**, 2913-2919.

BONSE, U. (1964). *Z. Phys.* **117**, 385-423.

CHUKHOVSKII, F. N. (1974). *Kristallografiya*, **19**, 482-488.

CHUKHOVSKII, F. N. (1981). *Metallofizika*, **3**, 3-30.

CHUKHOVSKII, F. N., GABRIELYAN, K. T. & PETRASHEN', P. V. (1978). *Acta Cryst.* A**34**, 610-621.

CHUKHOVSKII, F. N. & PETRASHEN', P. V. (1977). *Acta Cryst.* A**33**, 311-319.

GRONKOWSKI, J. & MALGRANGE, C. (1984). *Acta Cryst.* A**40**, 507-522.

HART, M. (1966). *Z. Phys.* **189**, 269-291.

KATO, N. (1964). *J. Phys. Soc. Jpn*, **19**, 971-985.

KHRUPA, V. I., KISLOVSKII, E. N. & DATZENKO, L. I. (1980). *Metallofizika*, **2**, 55-59.

KUSHNIR, V. I., SUVOROV, E. V. & MUKHIN, K. YU. (1980). *Fiz. Tverd. Tela*, **22**, 2135-2143.

MALGRANGE, C. (1969). *Acta Cryst.* A**25**, 356-363.

PENNING, P. (1966). *Philips Res. Rep. Suppl.* **21**, 1-113.

PETRASHEN', P. V. (1973). *Fiz. Tverd. Tela*, **15**, 3131-3132.

PETRASHEN', P. V. (1976). *Fiz. Tverd. Tela*, **18**, 3729-3731.

PETRASHEN', P. V. & CHUKHOVSKII, F. N. (1975). *Zh. Eksp. Teor. Fiz.* **69**, 477-487.

PETRASHEN', P. V., CHUKHOVSKII, F. N. & SHULPINA, I. L. (1980). *Acta Cryst.* A**36**, 287-295.

PETRASHEN', P. V. & YAROSLAVSKAYA, N. S. (1981). *Phys. Status Solidi A*, **68**, K15-K19.

SHULPINA, I. L., PETRASHEN', P. V., CHUKHOVSKII, F. N. & GABRIELYAN, K. T. (1984). Tezisi Dokl. IV. Vsesoyuz. Sovetch. Defecti Strukturi v Poluprovodnikakh, Novosibirsk 23-25 Oktyabr 1984, part 2, p. 114. (In Russian.)

Acta Cryst. (1988). A**44**, 14-17

A Rigorous Treatment of the Asymptotic Development of the Probability Density of a Structure Factor in $P\bar{1}$

BY J. BROSIUS

Université du Burundi, Département de Mathématiques, BP 2700, *Bujumbura, Burundi*

(*Received* 4 *November* 1986; *accepted* 1 *June* 1987)

Abstract

It is shown that an asymptotic development up to order N^{-2} exists for the density of the structure factor in $P\bar{1}$. An upper bound for the error is calculated.

1. Definitions

We shall consider the centrosymmetric case $P\bar{1}$. For N equal atoms and reciprocal-lattice vector $\mathbf{h}$,

$$E_{\mathbf{h}} = (2/N^{1/2}) \sum_{j=1}^{n} \cos(2\pi \mathbf{r}_j.\mathbf{h}) \quad (n = N/2)$$

is the normalized structure factor. Now let $\mathbf{x}_1, \mathbf{x}_2, \ldots, \mathbf{x}_n$ $(n = N/2)$ be n vectors that are distributed independently and uniformly over the unit cell and consider the random variable

$$\hat{E}_{\mathbf{h}} = 2N^{-1/2} \sum_{j=1}^{n} \cos(2\pi \mathbf{x}_j.\mathbf{h}) \quad (n = N/2). \quad (1)$$

Let us denote by $E \to p(E)$ the probability density of the random variable $\hat{E}_{\mathbf{h}}$.

2. Theorem

$$\begin{aligned} &|P(E) - (2\pi)^{-1/2}[\exp(-E^2/2)]\{1 - (1/8N)H_4(E) \\ &\quad + (1/N^2)[+(1/18)H_6(E) + (1/128)H_8(E)]\}| \\ &\quad \le [8/N^3(2\pi)^{1/2}](15{\cdot}2 + 22{\cdot}7/N + 195{\cdot}52/N^2 \\ &\qquad + 11\,217{\cdot}28/N^3) \\ &\qquad + (N^{1/2}/2\pi)[J_0(1)]^{(N/2)-4} \int_1^\infty |J_0(x)|^4 \, dx \\ &\qquad + (N^{1/2}/2\pi) \int_1^\infty \exp(-Nu^2/8) \, du \end{aligned} \quad (2)$$

where

$$\begin{aligned} H_4(E) &= E^4 - 6E^2 + 3 \\ H_6(E) &= E^6 - 15E^4 + 45E^2 - 15 \\ H_8(E) &= E^8 - 28E^6 + 210E^4 - 420E^2 + 105. \end{aligned} \quad (3)$$

0108-7673/88/010014-04$03.00